Development of finite element model using incremental endochronic theory for temperature sensitive material

Tienfuan Kerh† and Y. C. Lin‡

*Department of Civil Engineering, National Pingtung University of Science and Technology,
Pingtung 91207, Taiwan*

Abstract.   A novel finite element model based on the incremental endochronic theory with the effect of temperature was developed in this study to explore the deformed behaviors of a flexible pavement material. Three mesh systems and two loading steps were used in the calculation process for a specimen of three-dimensional circular cylinder. Computational results in the case of an uni-axial compression test for temperatures at 20ºC and at 40ºC were compared with available experimental measurements to verify the ability of developing numerical scheme. The isotropic response and the deviatoric response due to the thermal effect were presented from deformations in different profiles and displacement plots for the entire specimen. The characteristics of changing asphalt concrete material under a specified loading condition might be seen clearly from the numerical results, and might provide an useful information in the field of road engineering.

Key words: temperature sensitive material; endochronic theory; finite element method; isotropic response; deviatoric response.

1. Introduction

Temperature sensitive material such as asphalt concrete is frequently used as a pavement material in the field of road engineering. Due to flexible nature of the asphalt concrete, it requires a suitable model to describe the changing behavior of the material under loading conditions for helping a road designer from practical point of view. Indeed, there do exist many theoretical models for analyzing the mechanical behavior of a material, and which basically may include elastic model, hypo-elastic model, visco-elastic model, plastic model, and elastic-plastic model (e.g., AASHTO 1993, Henrinksen 1984, Kerh and Huang 1998, Liu 1993, Lu 1998, Lu and Pang 1995, Monismith 1992, Rowe *et al.* 1995, Sargious 1975, Uzan 1992, Wieckowski 2000, Yoon *et al.* 1999). Among these models, each one do have its own advantages and disadvantages, but the endochronic model based on plastic theory with a modification have been successfully derived and applied to describe the stress-strain behavior for the flexible pavement material.

From previous research papers, it can be found that the endochronic theory has mostly applied for metal, truss, composite and sand materials (e.g., Lee 1995, Peng and Ponter 1993a, 1993b, Sugiura

---

† Professor
‡ Graduate Student

et al. 1987, Valanis and Fan 1983, Wu *et al.* 1995, 1990, Wu and Aboutorabi 1988, Wu and Wang 1983, Wu *et al.* 1985, Wu and Sheu 1983, Wu and Aboutorabi 1988). The application of this method to asphalt concrete material is relatively less to see up to the present time; particularly, the finite element analysis in this topic is still opened in recent for researchers. Kerh and Huang (1998) conducted a work in this area; a finite element model based on the incremental endochronic theory for flexible pavement material has been developed. Reasonable agreement with the laboratory results has been shown in their study, but the effect of temperature was out of their consideration. As the asphalt concrete can be influenced significantly by the factor of temperature, it does deserve an attention to include the thermal effect in the model to further exploring more details in this interesting problem. Therefore, the objective of this study is mainly based upon the finite element method to develop a new numerical model including the effect of temperature in the incremental endochronic theory for describing the deforming behaviors of the flexible pavement material.

For developing a numerical model including the temperature effect for the flexible pavement material, it requires at first have a theoretical model for finite element formulation. Lu (1998), has derived a series of constitutive equations from the endochronic plasticity for this problem. The thermal factor was introduced in the most temperature sensitive parts of the constitutive equations, which are the bulk modulus and shear modulus, the hardening function, and the evolution equations for internal variables. Note that in particular the bulk modulus and shear modulus are no longer constants but a function of temperature. This model modification has shown to be very useful for describing the stress-strain behaviors for an asphalt concrete material under 40ºC, but the ability is decreased as the temperature getting higher. In spite of the disadvantage of this endochronic theory in high temperature conditions, this model might be sufficiently to provide an application in a general road temperature condition, and could be used as a theoretical background for the present study.

To further investigate the stress-strain characteristics of the flexible pavement material, in this study, the developed finite element model in line of the endochronic theory is taken to analyze the deformed behaviors of a three-dimension asphalt concrete specimen under a specified loading for both of temperatures at 20ºC and 40ºC. Three mesh generations and two loading steps are used in the calculation process to compare the obtaining solutions. Some of the computational results are compared with experimental measurements available in SHRP reports (Lytton and Roque 1991, Monismith *et al.* 1991) to demonstrate the ability of developing numerical scheme. Illustrations of the deforming body are presented in detail in accordance with the isotropic response and the deviatoric response obtained from the present finite element formulation. These numerical results may provide valuable information for a practical engineer in the design of flexible pavement structure.

2. Theoretical background of endochronic models with temperature factor

The endochronic theory can be categorized into two types rely on which model, Hemholtz free energy model or Gibbs free energy model, is employed in the formulation. Previous studies as reviewed in the above section have shown that the latter model is more suitable to analyze the mechanical behaviors of a flexible pavement material (Lu 1998, Lu and Pang 1995 and cited references). Thus, according to the Gibbs free energy, the basic stress controlled equation has the form:

$$\Phi = -\frac{1}{2}\sigma \cdot A \cdot \sigma - \sum_h \sigma \cdot B^h \cdot \gamma^h + \frac{1}{2}\sum_h \gamma^h \cdot E^h \cdot \gamma^h - \sum_s \sigma \cdot C^s \cdot P^s + \frac{1}{2}\sum_s P^s \cdot D^s \cdot P^s \tag{1}$$

where σ is the stress, γ^h and π^s represent the isotropic and deviatoric internal variables, with h and s are the total numbers of variables. Additionally, A, B, C, D, E are the fourth-order isotropic tensors. From this equation, a detailed deviation of stress-strain relationship and a series of constitutive equations of the endochronic models can be found in the above references. Here now by considering the thermal factor in three major parts of the constitutive equations, at first, assuming that the bulk modulus and shear modulus are not constant values but reasonable varied with the temperature, so the terms may be modified as:

$$K = K_{1h}(I_1 + I_0)^{-(K_{2h} \cdot T + K_{3h})} \tag{2}$$

$$G = K_{1d}(J_2 + J_0)^{-(K_{2d} \cdot T + K_{3d})} \tag{3}$$

where K_{1h}, K_{2h}, K_{3h}, K_{1d}, K_{2d}, K_{3d}, I_0, J_0 are material constants; T is the absolute temperature; I_1 and J_2 are the first invariant of stress and the second invariant of deviatoric stress. The above relationships make the bulk modulus and shear modulus decreasing its value with temperature nonlinearly.

From the stress-strain curve of asphalt concrete material in experimental results, it can be found that the tendency of curve varied with the temperature, which imply that the hardening function may consider as the second temperature sensitive part in the endochronic models. Then, the modified isotropic hardening function $h(\theta_{kk})$ and deviatoric hardening function $f(Z_D)$ may be written as:

$$h(\theta_{kk}) = \frac{c_h - (c_h - \theta_m)e^{-(\alpha_h \cdot T + \beta_h)\theta_{kk}}}{\theta_m - \theta_{kk}} \tag{4}$$

$$f(Z_D) = c_d - (c_d - 1)e^{-(\alpha_d \cdot T + \beta_d)Z_D} \tag{5}$$

where θ_{kk} is the maximum attainable plastic volumetric strain, and Z_D denotes the deviatoric intrinsic time, also the symbols c_h, α_h, β_h, c_d, α_d, β_d are material constants.

To account for the third temperature sensitive part, the increment of internal variables, $d\gamma_{kk}$ and dP_{ij} can be modified as:

$$d\gamma_{kk} = \left(\frac{B_0}{M_0(T)}\sigma_{kk} - \frac{E_0}{M_0(T)}\gamma_{kk}\right)dZ_H \tag{6}$$

$$dP_{ij} = \left(\left(\frac{C_0'\delta_{ij}}{N_0'(T)} + \frac{C_2}{N_2(T)}\right)S_{ij} - \left(\frac{D_0'\delta_{ij}}{N_0'(T)} + \frac{D_2}{N_2(T)}\right)P_{ij}\right)dZ_D \tag{7}$$

where

$$M_0(T) = M_{0a} \cdot T + M_{0b} \tag{8}$$

$$\frac{C_0}{N_0(T)} = \frac{C_0'}{N_0'(T)} + \frac{C_2}{N_2(T)}, \qquad \frac{D_0}{N_0(T)} = \frac{D_0'}{N_0'(T)} + \frac{D_2}{N_2(T)} \tag{9}$$

$$N_0(T) = N_{0a}e^{-N_{0b}(T-273)} + N_{0c}, \qquad N_2(T) = N_{2a}e^{-N_{2b}(T-273)} + N_{2c} \tag{10}$$

and where C_0, C_2, D_0, D_2, M_{0a}, M_{0b}, N_{0a}, N_{0b}, N_{0c}, N_{2a}, N_{2b}, N_{2c} are constants associated with the corresponding equations or material parameters.

3. Development of finite element models with temperature effect

As introduced in previous section, the governing constitutive equations based on the endochronic theory may be divided into the isotropic portion and the deviatoric portion. Here now in this section the finite element method is applied to develop a numerical model for analyzing changing behaviors of the flexible pavement material. For the incremental isotropic response, the equation is:

$$d\varepsilon_{kk} = \frac{1}{3K}d\sigma_{kk} + 3B_0 d\gamma_{kk} \tag{11}$$

where $d\sigma_{kk}$ is the increment of isotropic stress, $d\varepsilon_{kk}$ is the increment of isotropic strain, and $d\gamma_{kk}$ is the internal variable for isotropic deformation. If the thermal factor is considered in the internal variable, the above equation then becomes:

$$d\sigma_{kk} = 3K d\varepsilon_{kk} - 9KB_0\left(\frac{B_0}{M_0(T)}\sigma_{kk} - \frac{E_0}{M_0(T)}\gamma_{kk}\right)dZ_H \tag{12}$$

For the incremental deviatoric response, the equation is:

$$de_{ij} = \frac{1}{G}dS_{ij} + C_1 dP_{ij} \tag{13}$$

where dS_{ij} represents the increment of deviatoric stress, and de_{ij} denotes the increment of deviatoric strain. From the definitions and by introducing the temperature factor, the equation can be derived as follows:

$$d\sigma_{ij} = G d\varepsilon_{ij} + \left(K - \frac{G}{3}\right)d\varepsilon_{kk}\delta_{ij} - 3KB_0\left(\frac{B_0}{M_0(T)}\sigma_{kk} - \frac{E_0}{M_0(T)}\gamma_{kk}\right)dZ_H\delta_{ij} - GC_1 dP_{ij} \tag{14}$$

To employ the finite element method properly (e.g., Fagan 1992, Moaveni 1999), the above equation must be converted to a matrix form as:

$$\{d\sigma\}_{6\times1} = [D]_{6\times6}\{d\varepsilon\}_{6\times1} + \{dHP\}_{6\times1} \tag{15}$$

where the stress vector and the strain vector are:

$$\{d\sigma\}^T = \{d\sigma_{xx}, \ d\sigma_{yy}, \ d\sigma_{zz}, \ d\sigma_{xy}, \ d\sigma_{xz}, \ d\sigma_{yz}\} \tag{16}$$

$$\{d\varepsilon\}^T = \{d\varepsilon_{xx}, \ d\varepsilon_{yy}, \ d\varepsilon_{zz}, \ d\varepsilon_{xy}, \ d\varepsilon_{xz}, \ d\varepsilon_{yz}\} \tag{17}$$

In addition to the temperature effect, the symmetric transformation matrix $[D]$ and the force vector $\{dHP\}$ can be derived from Eqs. (14) and (15) and thus the complete forms for these matrix and vector are:

$$[D]_{6\times 6} = \begin{bmatrix} K+\dfrac{2G}{3} & K-\dfrac{G}{3} & K-\dfrac{G}{3} & 0 & 0 & 0 \\[6pt] K-\dfrac{G}{3} & K+\dfrac{2G}{3} & K-\dfrac{G}{3} & 0 & 0 & 0 \\[6pt] K-\dfrac{G}{3} & K-\dfrac{G}{3} & K+\dfrac{2G}{3} & 0 & 0 & 0 \\[6pt] 0 & 0 & 0 & G & 0 & 0 \\[4pt] 0 & 0 & 0 & 0 & G & 0 \\[4pt] 0 & 0 & 0 & 0 & 0 & G \end{bmatrix} \tag{18}$$

and

$$\{dHP\}_{6\times 1} = \left\{ \begin{array}{c} -3B_0\left[k_{1h}(I_0+I_1)^{-(k_{2h}T+k_{3h})}\right]\left[\left(\dfrac{B_0}{M_0(T)}\sigma_{kk}-\dfrac{E_0}{M_0(T)}\gamma_{kk}\right)dZ_H\right] \\[10pt] -3B_0\left[k_{1h}(I_0+I_1)^{-(k_{2h}T+k_{3h})}\right]\left[\left(\dfrac{B_0}{M_0(T)}\sigma_{kk}-\dfrac{E_0}{M_0(T)}\gamma_{kk}\right)dZ_H\right] \\[10pt] -3B_0\left[k_{1h}(I_0+I_1)^{-(k_{2h}T+k_{3h})}\right]\left[\left(\dfrac{B_0}{M_0(T)}\sigma_{kk}-\dfrac{E_0}{M_0(T)}\gamma_{kk}\right)dZ_H\right] \\[10pt] 0 \\[4pt] 0 \\[4pt] 0 \end{array} \right\}$$

$$-\left\{ \begin{array}{c} C_1\left[k_{1d}(J_2+J_0)^{-(k_{2d}T+k_{3d})}\right]\left(\dfrac{C_0}{N_0(T)}S_{11}-\dfrac{D_0}{N_0(T)}P_{11}\right)dZ_D \\[10pt] C_1\left[k_{1d}(J_2+J_0)^{-(k_{2d}T+k_{3d})}\right]\left(\dfrac{C_0}{N_0(T)}S_{22}-\dfrac{D_0}{N_0(T)}P_{22}\right)dZ_D \\[10pt] C_1\left[k_{1d}(J_2+J_0)^{-(k_{2d}T+k_{3d})}\right]\left(\dfrac{C_0}{N_0(T)}S_{33}-\dfrac{D_0}{N_0(T)}P_{33}\right)dZ_D \\[10pt] C_1\left[k_{1d}(J_2+J_0)^{-(k_{2d}T+k_{3d})}\right]\left(\dfrac{C_0}{N_0(T)}S_{12}-\dfrac{D_0}{N_0(T)}P_{12}\right)dZ_D \\[10pt] C_1\left[k_{1d}(J_2+J_0)^{-(k_{2d}T+k_{3d})}\right]\left(\dfrac{C_0}{N_0(T)}S_{13}-\dfrac{D_0}{N_0(T)}P_{13}\right)dZ_D \\[10pt] C_1\left[k_{1d}(J_2+J_0)^{-(k_{2d}T+k_{3d})}\right]\left(\dfrac{C_0}{N_0(T)}S_{23}-\dfrac{D_0}{N_0(T)}P_{23}\right)dZ_D \end{array} \right\} \tag{19}$$

From the principle of virtual work, it states that the volume integral of the element stress multiple by a virtual strain is equal to the element external force multiple by a virtual displacement. Therefore, the equation for an element in matrix form can be obtained as:

$$\iiint_V [B]^T [D][B]dV\{du\} = \{dP\} - \iiint_V [B]^T \{dHP\}dV \tag{20}$$

where $\{du\}$ is the displacement vector, $\{dP\}$ is the external force on the element, and V is the volume of the element. Furthermore, $[B]$ denotes the strain-displacement relationship matrix, which can be calculated from shape functions of the chosen element. After assembly for the entire elements, the above global equation can finally be simplified as:

$$[K]\{du\} = \{dP\} - \{dPF\} \tag{21}$$

where the stiffness matrix $[K] = \iiint_V [B]^T [D][B]dV$ and the plastic pseudo-force vector $\{dPF\} = \iiint_V [B]^T \{dHP\}dV$ are obtained on an element basis. In each element, the corresponding matrix or vector can be evaluated by using Gauss quadrature. After prescribed boundary conditions, the resulting global system of equations can then be calculated by direct numerical method.

4. Verification and illustration of numerical results

   To perform the finite element calculation and to comply with experimental conditions, consider now a circular cylinder of 4 inches in diameter and 4 inches in height. As it has a symmetric shape, only one half of the cylinder is taken for analysis, and three mesh systems mesh1, mesh2 and mesh3 are used to divide the specimen. Shown in Fig. 1 is the example for mesh3 system, where there are 6×6 elements in X-Y plane, and there are 3 elements equally arranged in Z-component. Hence, a total of 108(196 nodes) cubic eight-node isoparametric elements is included in this mesh, which is the finest grid used for computation in this study if compared with two other mesh systems, mesh1 $(4 \times 4 \times 3)$ and mesh2 $(6 \times 6 \times 2)$, which have 48(100) and 72(147) elements (nodes), respectively.
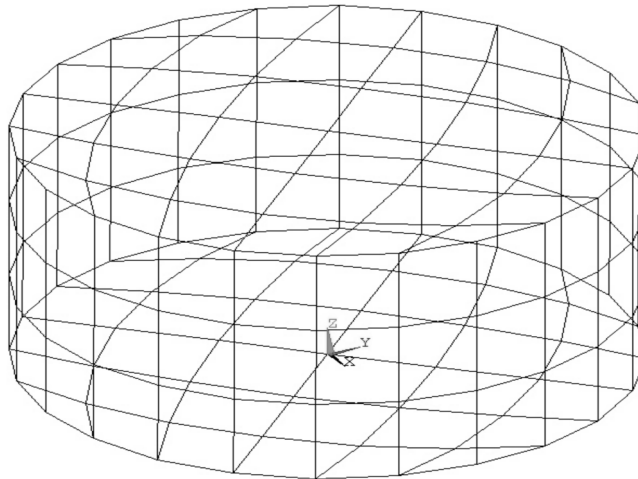

Fig. 1 Mesh generation of the circular cylinder specimen (mesh3 system)

For the boundary conditions, the deformations in X and Y directions are constrained on nodes of the top surface elements, but only Z-component is confined on each node of the bottom surface element. For the side boundary, free conditions are applied to find out the tendency of calculation results. In these conditions, the top surface element (Z = 2) is contacted with a portion of compression test equipment, so that the contact surface may consider as supported by a hinge and no deformations are allowed in X and Y components, which may imply that significant friction force exists on the top platen of the test machine. As indicated above, the whole cylinder has a symmetrical shape (4 inches in total height, Z = −2 to 2), the present finite element computation is taken only a half of the specimen (2 inches in height, Z = 0 to 2) for modeling the problem. That is, the bottom surface (Z = 0) in here is the center surface of the whole cylinder in Z-direction, which is not the contact surface between specimen and compression test machine. Thus, the boundary conditions in this element surface are set to zero deformations in Z-component due to symmetrical behavior. This corresponds to the existence of friction force for the whole specimen but zero values on this neutral surface. These boundary conditions are reasonable as they do not violate the physical meanings of boundary condition prescribed on the top platen.

Note that before go for the computation, it requires to determine the several material parameters, which may be obtained by curve fitting the experimental data (Lytton and Roque 1991, Monismith *et al.* 1991). Further to say is that by comparing the obtained stress-strain curve from theory with available experimental data, and when the theoretical curve is in consistent with the result of experiments, the resulting constants are then determined for both of isotropic and deviatoric parts, where hydrostatic compression test and triaxial test are used for both parts respectively. As the present finite element models are developed on the basis of endochronic theory, the choice of material parameters can be taken directly from the theoretical report (Lu 1998), who has described the details of obtaining these material constants using various theoretical equations. Therefore, for the isotropic portion, the material constants are: $\alpha_h = -5/°K$, $\beta_h = 1905$, $\theta_m = 0.00255$, $k_1 = 0.9$, $k_{1h} = 50000$, $k_{2h} = 0.0052/°K$, $k_{3h} = -1.85$, $B_0 = 0.47$, $c_h = 2.1$, $E_0 = 100$ KPa, $I_0 = 1000$ KPa, $M_{0a} = -0.005$ KPa/°K, $M_{0b} = 2.57$ KPa. For the deviatoric portion, the constants are: $\alpha_d = 100/°K$, $\beta_d = -26770$, $C_0 = 0.526$, $C_2 = 0.526$, $C_d = 10$, $D_0 = 600$ KPa, $D_2 = 600$ KPa, $J_0 = 50$ KPa, $K_2 = 0.75$, $K_{1d} = 400000$, $K_{2d} = 0.0015/°K$, $K_{3d} = -0.37$, $N_{0a} = 183$, $N_{0b} = 0.068$, $N_{0c} = 13$, $N_{2a} = 825$ KPa, $N_{2b} = 716/°K$. $N_{2c} = 1.1$ KPa. With these curve fitting material constants, some have units but some are not as shown above, the numerical computation can be performed and the results are presented in the next discussions.

For verification of the present finite element models, the computational results compared with theoretical solutions and SHRP experimental measurements of an uni-axial compression test are exhibited in Figs. 2 and 3 for different cases of temperature. From the stress-strain curves, it can be seen that reasonable good agreements are achieved for both of temperature conditions, and the accuracy of computational results is improved as the element number is increased, i.e. mesh3 obtained the most accurate results which comply with the basic principle of finite element method. Additionally, if a statistical *t*-test is performed for results of mesh3 system and experiment, it can be find that the former temperature case has $t = -2.12$, and the latter temperature case has $t = 2.1$. Both tests are within the acceptance intervals $-2.3646 < t < 2.3646$ and $-2.2622 < t < 2.2622$, with significance level $\alpha = 0.05$, for degree of freedoms $v = 7$ and $v = 9$, respectively. These tests may further to enhance the reliability of the present numerical results.

To further check the effect of loading steps in the calculation process, consider the uniform axial stress *p* on the specimen is divided into 300 and 600 loading steps; that is, the increment of loading
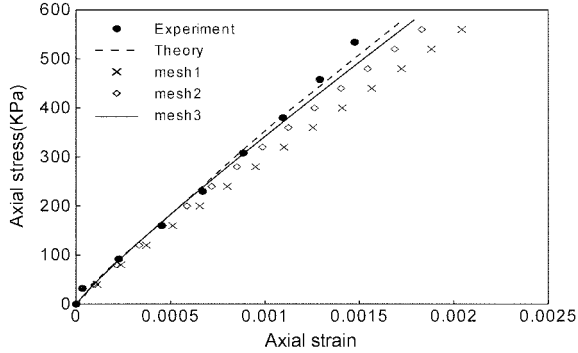
Fig. 2 Comparison of finite element solutions with theoretical and experimental results ($T = 20°C = 293°K$)
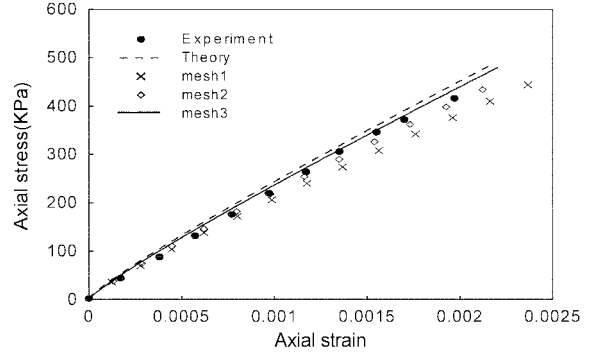

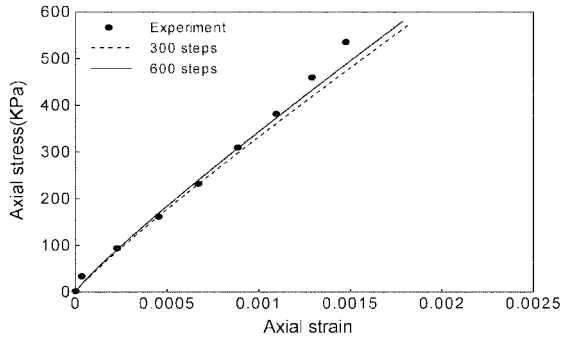Fig. 3 Comparison of finite element solutions with theoretical and experimental results ($T = 40°C = 313°K$)

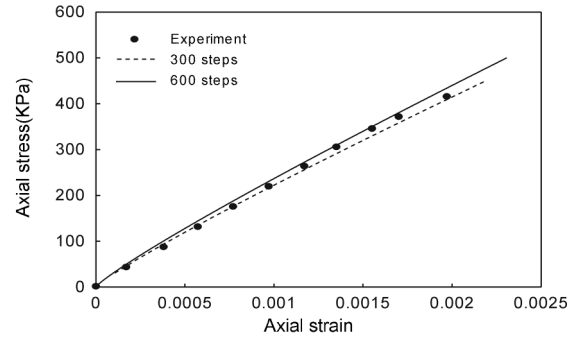

Fig. 4 Comparison of loading steps in the calculation process ($T = 20°C = 293°K$)

Fig. 5 Comparison of loading steps in the calculation process ($T = 40°C = 313°K$)

in each step is $p/300$ and $p/600$ for the two cases. Then, the values of strain can be obtained from numerical calculation, and shown in Figs. 4 and 5 are the computational stress-strain curves for the two temperatures. These comparisons proved that the more loading steps the more reliable results may be expected, but the computational cost may also be increased.

As presented in the above illustrations, the mesh3 system and the 600 loading steps employed in this study can obtain results of sufficiently numerical accuracy, so the same conditions will be used for analyzing more details of deforming behavior for the asphalt concrete material. Due to three cubic elements are equally divided the specimen in Z-direction as seen in the finest mesh system, the nodal solutions in four profiles (Z = 2.0, 4/3, 2/3, 0) thus can be taken for describing the behaviors of the deformed material under a specified loading. By taking the case of temperature 40°C as an example, exhibited in Fig. 6 is the isotropic response in the X-Y plane for these four profiles, and a symmetric deformation is seen for the four profiles. Whereas, when the deviatoric response is included in the plots as shown in Fig. 7, owing to the added pseudo-force or friction force is not zero at each incremental calculation of the internal variables, the deforming behavior becomes a non-symmetric pattern for the four profiles. In both figures, it also can be seen that the fourth profile has higher deformation than the other profiles due to the effect of compression.
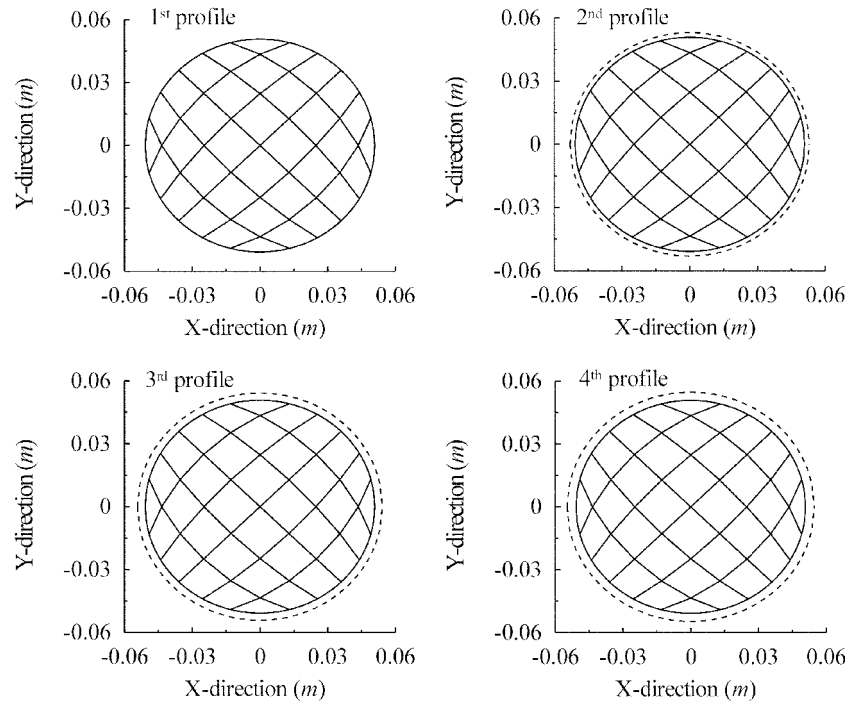
Fig. 6 Deformation of each profile due to the isotropic effect ($T = 40^{\circ}C = 313^{\circ}K$)

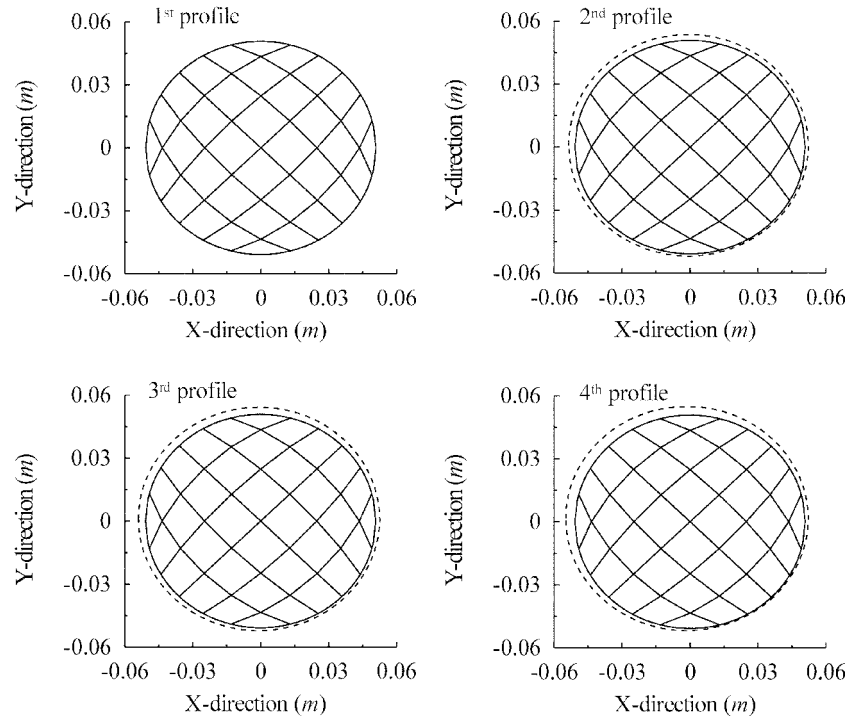Fig. 7 Deformation of each profile due to the isotropic and deviatoric effects ($T = 40^{\circ}C = 313^{\circ}K$)

```
.332E-19
.179E-04
.358E-04
.537E-04
.716E-04
.895E-04
.107E-03
.125E-03
.143E-03
```
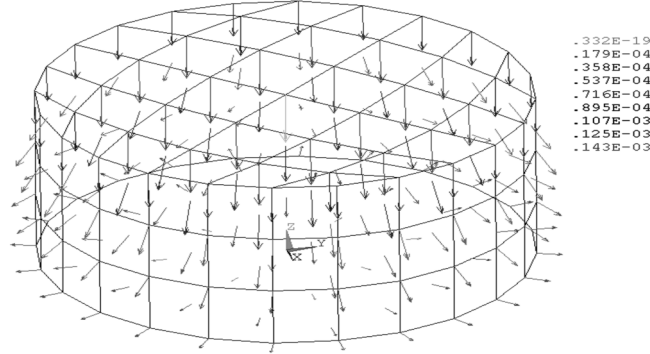
Fig. 8 Three-dimensional displacement plot of the isotropic response ($T = 40$ºC $= 313$ºK, unit: *m*)


```
.687E-19
.208E-04
.416E-04
.623E-04
.831E-04
.104E-03
.125E-03
.145E-03
.166E-03
```
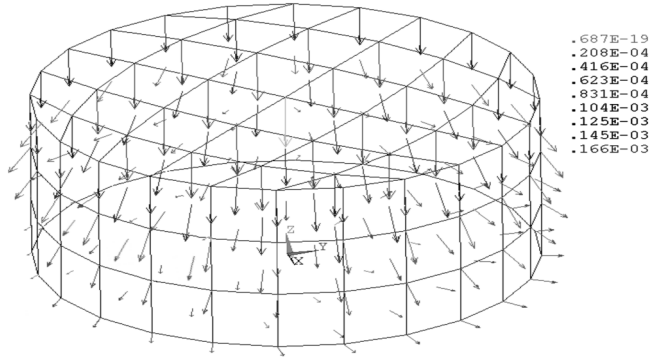
Fig. 9 Three-dimensional displacement plot of the isotropic and deviatoric responses ($T = 40$ºC $= 313$ºK, unit: *m*)

To view more clearly in each nodal deformation, three-dimensional displacement plots, including both of isotropic response and deviatoric response, for the entire specimen are shown in Figs. 8 and 9. From the boundary conditions for both figures, only deformation in Z-direction is observed in the top profile, but in the bottom profile, no deformation in Z-direction is seen due to the applied constraint conditions. Again, these 3-D displacement plots clearly to show that the isotropic response has a symmetric behavior, but a tendency of non-symmetric behavior is occurred for the deviatoric response. These detailed deformation analysis of the flexible pavement material under a specified loading condition may help engineer to understand more about the characteristics of an asphalt concrete and may provide an useful information for a road designer.

Note that a perfect material does not exist from practical point of view; in particular, the asphalt concretes mainly consist of sand, gravel and asphalt mixtures. As the size and the shape of each particle can never be the same, so it is non-uniformly distributed in usual for a test specimen. As a result, the non-symmetrical mechanical behavior more or less may be existed even the experimental measurement is controlled within very strictly conditions. From some engineering aspects, the deviation of material behavior is out of importance, as it does not affect the global results significantly. However, theoretically we like to develop a model and try to describe its changing behavior more precisely. In the present study, the deviatoric part of the endochronic plastic theory is one of the methods to approach this problem. In each incremental calculation step, if the deviatoric internal variable dP_{ij} is set to zero in Eqs. (13) and (14), then the computational results have symmetrical shapes

as presented in Figs. 6 and 8, respectively On the other hand, although the external compression force on the top boundary surface of the specimen can be equally distributed to each node of the element, when $dP_{ij} \neq 0$, the non-zero friction force or pseudo-force $\{dPF\}$ which calculated from $\{dHP\}$ in Eqs. (19) and (21), may not be equally applied in each node of the elements locally, and thus obtained non-symmetrical deformations as shown in Figs. 7 and 9, respectively.

Besides, the deviatoric material constants employed in this study are basically gained from curve fitting the available experimental data. According to the endochronic theory, three tests including volumetric compression test, pure shear test and deviatoric test may be required for corresponding to isotropic response, deviatoric response in non-axial direction and deviatoric response in axial direction. But in reality, the deviatoric test is not easy to perform directly for a flexible pavement material, and thus the simplest way to obtain its data is by using the subtraction result of uni-axial test (non-pure axial direction) and the volumetric compression test (pure axial direction). Since the measurements can never be perfect due to any reason, and the error of data set usually is acceptable within a reasonable range. Therefore, the post-calculation in the developed finite element model may also be expected to obtain some deviations in the deformations. In addition, the direction of non-symmetrical deformed behavior is not a major concern as the specimen studied in this study has a circular profile, and the result makes no difference for the properly defined coordinate system.

5. Conclusions

The flexible pavement material such as asphalt concrete is significantly influenced by the variation of temperature. Based on the endochronic plasticity theory with the effect of temperature, a series of constitutive equations have been derived by previous researchers for describing its stress-strain behaviors. However, the application of numerical method to this crucial issue was relatively less to see up to the present time. Therefore, in this study, a new incremental governing equation has been developed by the application of finite element method to the endochronic theory with the consideration of thermal factor. Three mesh systems have been used in the calculations to check the grid independence, and two loading steps have been compared to check their influence on the solutions. The computational results for the case of an uni-axial compression test at temperatures 20°C and 40°C have compared with experimental measurements available in SHRP reports to verify the accuracy of the present numerical model. Then, the isotropic response and the deviatoric response of a specimen under uniform pressure condition have properly described from various plots of different deformation profiles and 3-D displacements. The results have shown that a symmetric deformation was observed for the isotropic response, but if the deviatoric response is included in the analysis, a non-symmetric deformation pattern was occurred due to the plastic pseudo-force is not zero at each incremental calculation of the internal variables. The analyzing results might provide valuable information for a practical engineer in the design of flexible pavement material.

References

AASHTO (1993), "Guide for design of pavement structure", American Association of State Highway and Transportation Officials, Washington D.C., USA.

Fagan, M.J. (1992), *Finite Element Analysis, Theory and Practice*, Longman Scientific and Technical, UK.

Henriksen, M. (1984), "Nonlinear viscoelastic stress analysis - A finite element approach", *Comput. Struct.*, **18**(1), 133-139.

Kerh, T. and Huang, C.Y. (1998), "Finite element application of an incremental endochronic model to flexible pavement materials", *Struct. Eng. Mech.*, **6**(7), 817-826.

Lee, C.F. (1995), "Recent finite element applications of the incremental endochronic plasticity", *Int. J. Plasticity*, **11**(7), 843-865.

Liu, M.L. (1993), "The structure response of pavement by using the hypoelastic model", *The 17th Nat. Conf. Theo. Appl. Mech.*, Taiwan, 761-768.

Lu, J.K. (1998), "The endochronic model for temperature sensitive materials", *Int. J. Plasticity*, **14**(10-11), 997-1012.

Lu, J.K. and Pang, C. (1995), "Plasticity model of the mechanical behavior for an asphalt concrete", *J. Taiwan Highway Eng.*, **21**(11/12), 58-64.

Lytton, R.L. and Roque, R. (1991), "Performance-models and validation of test results", *SHRP report A-005*, Texas. Transportation Institute, Texas A&M University, TX, USA.

Moaveni, S. (1999), *Finite Element Analysis, Theory and Application with ANSYS*, Prentice-Hall, Inc., USA.

Monismith, C.L. (1992), "Analytically based asphalt pavement design and rehabilitation: Theory and practice", *TRB 1354*, 5-26.

Monismith, C.L., Hick, R.G. and Finn, F.N. (1991), "Performance-related testing and measuring of asphalt-aggregate interaction and mixtures", *SHRP Report A-003*, Institute of Transportation Studies, U. C. Berkeley, CA, USA.

Peng, X. and Ponter, A.R.S. (1993a), "Extremal properties of endochronic plasticity, Part I: Extremal path of the constitutive equation with a yield surface", *Int. J. Plasticity*, **9**, 551-566.

Peng, X. and Ponter, A.R.S. (1993b), "Extremal properties of endochronic plasticity, Part II: Extremal path of the constitutive equation with a yield surface and application", *Int. J. Plasticity*, **9**, 567-581.

Rowe, G.M., Brown, S.F. and Bouldin, M.J. (1995), "Visco-elastic analysis of hot mix asphalt pavement structures", *Transportation Research Board 74th Annual Meeting*, Washington D.C., Paper No. 95-0617.

Sargious, M. (1975), *Pavement and Surfacing for Highways and Airports*, Applied Science Pub. Ltd., England.

Sugiura, K., Lee, G.C. and Chang, K.C. (1987), "Endochronic theory for structures steel under nonproportional loading", *J. Eng. Mech.*, **113**(12), 1901-1917.

Uzan, J. (1992), "Resilient characterization of pavement materials", *Int. J. Numerical Analytical Methods in Geomechanics*, **16**, 453-549.

Valanis, K.C. and Fan, J. (1983), "Endochronic analysis of cyclic elastoplastic strain fields in a notched plate", *J. Appl. Mech.*, Transactions of the ASME, **50**, 789-974.

Wieckowski, Z. (2000), "Dual finite element methods in homogenization for elastic-plastic fibrous composite material", *Int. J. Plasticity*, **16**, 199-221.

Wu, H.C., Hong, H.K. and Lu, J.K. (1995), "An endochronic theory accounted for deformation induced anisotropy", *Int. J. Plasticity*, **11**(2), 145-162.

Wu, H.C., Wang, P.T., Pan, W.F. and Xu, Z.Y. (1990), "Cyclic stress-strain response of porous aluminum", *Int. J. Plasticity*, **6**, 207-230.

Wu, H.C. and Aboutorabi, M.R. (1988), "Endochronic modeling of coupled volumetric-deviatoric behavior of porous and granular materials", *Int. J. Plasticity*, **4**, 163-181.

Wu, H.C. and Wang, T.P. (1983), "Endochronic description of sand response to static loading", *J. Eng. Mech.*, ASCE, **109**, 970-987.

Wu, H.C., Wang, Z.K. and Aboutorabi, M.R. (1985), "Endochronic modeling of sand in true triaxial test", *J. Eng. Mech.*, **111**(10), 1257-1276.

Wu, H.C. and Sheu, J.C. (1983), "Endochronic modeling for shear hysteresis of sand", *J. Geotechnical Eng.*, **109**(12), 1539-1550.

Wu, H.C. and Aboutorabi, M.R. (1988), "Endochronic model of sand with circular stress", *J. Geotechnical Eng.*, **114**(1), 93-103.

Yoon, J.W., Yang, D.Y., Chung, K. and Barlat, F. (1999), "A general elasto-plastic finite element formulation base on incremental deformation theory for planar anisotropy and its application to sheet metal forming", *Int. J. Plasticity*, **15**, 35-67.